A 2-D Observer to Estimate the Reaction Rate in a Stopped Flow Fixed Bed Reactor for Gas Phase Olefin Polymerization

Barbara Browning
Laboratoire de Génie des Procédés Catalytiques (LGPC), Université de Lyon, CPE Lyon, CNRS, UMR5285,43, Boulevard du 11 Novembre 1918, F-69616 Villeurbanne, France

Laboratoire de Chimie, Catalyse, Polymères et Procédés (C2P2), Université de Lyon, Univ. Lyon 1, CPE Lyon, CNRS, UMR 5265, LCPP group, 43, Boulevard du 11 Novembre 1918, F-69616 Villeurbanne, France

Nida Sheibat-Othman
Laboratoire d'Automatique et de Génie des Procédés (LAGEP), Université de Lyon, Univ. Lyon 1, CPE Lyon, CNRS, UMR 5007, 43, Boulevard du 11 Novembre 1918, F-69616 Villeurbanne, France

Isabelle Pitault
Laboratoire de Génie des Procédés Catalytiques (LGPC), Université de Lyon, CPE Lyon, CNRS, UMR5285,43, Boulevard du 11 Novembre 1918, F-69616 Villeurbanne, France

Timothy F. L. McKenna
Laboratoire de Chimie, Catalyse, Polymères et Procédés (C2P2), Université de Lyon, Univ. Lyon 1, CPE Lyon, CNRS, UMR 5265, LCPP group, 43, Boulevard du 11 Novembre 1918, F-69616 Villeurbanne, France

DOI 10.1002/aic.14538
Published online July 5, 2014 in Wiley Online Library (wileyonlinelibrary.com)

A two-dimensional high gain observer has been constructed to estimate the reaction rate parameters in a laboratory scale stopped flow fixed bed reactor for gas phase ethylene polymerization. The observer is based on the heat balances of a validated model of the reactor and the measured variable is the outlet temperature of the fixed bed. To create an observable system of equations, the polymerization rate is considered in two parts, an activation energy term and a lumped parameter. The effective radial conductivity in the fixed bed and the heat-transfer coefficient at the wall are considered separately. The polymerization rate is calculated from the observer results and is in good agreement with the measured data and calculated values. © 2014 American Institute of Chemical Engineers *AIChE J*, 60: 3511–3523, 2014
Keywords: state estimator, reactor modeling, olefin polymerization, nascent polymerization

Introduction

In this work, a stop flow ethylene polymerization reactor is considered, with limited temperature measurements. In industry, gas phase polymerization of ethylene is carried out in fluidized bed reactors using supported catalysts, most commonly Ziegler–Natta, $TiCl_4$ dispersed on $MgCl_2$, or chromium, CrO_x dispersed on silica.[1] However, such reactors do not allow study of the early stage of the reaction where a number of critical phenomena take place, such as the breakup of the catalyst support and rapid changes in the physical properties of the growing polymer chains.[2,3] Not only is the process dependant on the catalyst breakup occurring in a controlled manner but also the morphology of the final polymer particles is determined at this early stage while particle scale heat- and mass-transfer resistances are at a maximum due to the small external surface area of the initial catalyst. To study these effects, a packed bed reactor for the study of the first instants of gas phase polyolefin polymerization was designed and optimized.[4,5] The reactor was designed to perform experiments of very short and precise timescales at close to industrial conditions with relative gas flow rates similar to those experienced by the particles in a fluidized bed reactor. To use this reactor effectively, a good knowledge of the temperature profile in the reactor bed is needed. To gain this information a dynamic reactor model was constructed and validated, full details of which are given in previous work.[6]

The objective of this work is to estimate the ethylene consumption rate and the heat generated by the reaction throughout the stopped flow reactor. However, some reactor characteristics should be taken into account: the reaction rate is strongly nonlinear and highly exothermic leading to steep temperature profiles; and the bed is axially and radially distributed which gives a two-dimensional (2-D) distributed model with interactions between the sections. The estimate of the reaction rate, independent of the catalyst used, can be made using an observer. To our knowledge, the application of observers in 2-D distributed systems has never been considered for chemical engineering applications. Moreover,

Correspondence concerning this article should be addressed to N. Sheibat-Othman at nida.othman@lagep.cpe.fr.

temperature is only measured at two locations, and concentration is known only at the reactor inlet from the feed composition.

The use of observers has demonstrated its interest for monitoring and control of chemical processes. A number of state estimation methods are available for linear or nonlinear systems described by ordinary differential equations (ODEs; e.g., Kalman filter, high gain observer, H_∞ filter). However, most practical industrial processes are inherently distributed in space and time, and, therefore, are usually described by a set of nonlinear partial differential equations (PDEs) with a limited number of available measurements. In the usual estimation method for spatially distributed systems with a limited number of measurements, the first step is to spatially discretise the PDEs process model to obtain an approximate ODE representation, and then known observers for ODEs are applied. More recently, observers have also been proposed to reconstruct the infinite dimensional field as, for instance, the backstepping design observer.[7]

Most chemical engineering observer applications for estimation of process conditions still use methods, where the PDE model is discretized to ODEs before the observer is applied. For instance, based on spatial discretization of the PDE of a high-temperature metallurgical reactor, Lebreux et al.[8] used an unscented Kalman filter to estimate the ledge thickness on the walls. Aguilar-Garnica et al.[9] used the method of characteristics to discretise the PDE model of a plug flow reactor and then applied an interval observer for reactant concentration. Dochain[10] developed an exponential observer for nonisothermal fixed bed reactors, where the model was discretized using the finite difference method. Hua et al.[11] estimated the concentration profiles in a fixed bed reactor from inlet concentration and temperature measurements from a limited number of temperature sensors using a discretized model. A one-dimensional (1-D) model, assuming no temperature difference between catalyst particles and gas phase as well as negligible radial temperature gradient was considered. Wu and Li[12] proposed an adaptive neural observer for a class of parabolic PDE systems reformulated as ODEs and applied it for the estimation of the temperature profile for a catalytic rod.

Note that in a number of other applications for which similar ODE observers were applied, the PDE represents a gradient or range in the product quality, and not the reactor conditions. For instance Mangold et al.[13] proposed an observer for particle size in precipitation reactions, Edouard et al.[14] estimated the particle-size distribution in emulsion polymerization using a high gain observer and Zhang et al.[15] used a high gain observer to estimate the zeroth moment of the crystal size distribution, which is then controlled using the reactor temperature. Using the method of moments approximates the PDE to a very small number of ODEs, but is out of the scope of this work.

The construction of an estimator assumes the system is observable. However, besides transport dynamics, the observability of the model depends on the number, type, and location of sensors. Therefore, a number of works have studied the effect of sensor location on system observability. Vande Wouwe et al.[16] developed a sensor location criterion for either state estimation or parameter estimation. In Alonso et al.[17] the most appropriate sensor type and locations are chosen through a guided search algorithm that minimizes orthonormality distortion, using a low dimensional representation of the original distributed system. As the system observability also depends on the inputs, Kreuzinger et al.[18] indicate that simulation is the best way to investigate the system dynamics to deduce reasonable sensor locations and appropriate simplifications. They implemented their results together with an unscented Kalman filter or a Luenberger structure observer to monitor a stratified storage tank. As will be detailed later, in this work, temperature sensors are available at the reactor inlet and outlet, and in the hot water bath external to the reactor wall and the reactor exit gas flow rate is measured online.

The article is organized as follows: first of all, the reactor model is presented together with the experimental setup. Then, the theoretical background of the chosen observer is given. Two different forms of observer are then developed, using 1-D and 2-D discretized models. Finally, the observer results are compared to experimental data.

Reactor Setup and Model

Description of experimental setup

The laboratory scale, stainless steel, fixed bed reactor contains a mixture of catalyst, and inert solid (see Tioni et al.[5] for details of the reactor preparation and setup). The bed is 1 cm long by 2 cm diameter and is held in place by two 15 μm, stainless steel frits of thickness 3 mm. The reactor is equipped with two 1 mm T-type thermocouples, one at the inlet chamber and one at the exit chamber. It has a wall thickness of 1 cm and is plunged into a water bath that fixes the external temperature.

The reaction gas is a mixture of 67 % mol ethylene and 33 % mol helium. The gas is supplied to the reactor at 9×10^5 N m^{-2} via a pressure control valve and then heated by passage through the coils in the hot water bath operated at 353 K; the flow rate is measured at the reactor exit. The inert solid is NaCl and the supported catalyst (average particle diameter 58 μm) comprises 3–5 % wt of the bed. A computer controlled automatic valve, maintained at 353 K by electrical resistance, is set to open and close for a preset time period fixing the reaction duration. The reaction is stopped by rapid degassing followed by an injection of CO_2 via another automatic valve. Temperature data are collected automatically from the thermocouples. The process flow diagram of the reactor and setup is shown in Figure 1.

The recorded dataset for each experiment includes: online inlet and outlet temperatures, reactor exit gas flow rate, and offline final masses of catalyst, inert, and polymer formed. Typical measurements for an experiment of duration 15 s are shown in Figure 2. The short reaction time means a significant proportion of the heat produced exits the reactor during cooling, and so, this period is included in the model, but will not be useful for the observer as the reaction is stopped.

Reactor model

Ethylene polymerization is highly exothermic; the enthalpy of reaction is about 800–900 kcal/kg which is higher than most monomers. The reaction rate is rapid and depends on the catalyst used and the operating conditions. For a reaction rate of 2500 g g^{-1} h^{-1}, reported in grams of polymer formed per gram of catalyst per hour, the power generated in our reactor might attain 100 W, so overheating is a risk in the very early stages of the process. For this reactor, interparticle and interphase heat transfer limitations were evaluated based on the maximum observed reaction rate in

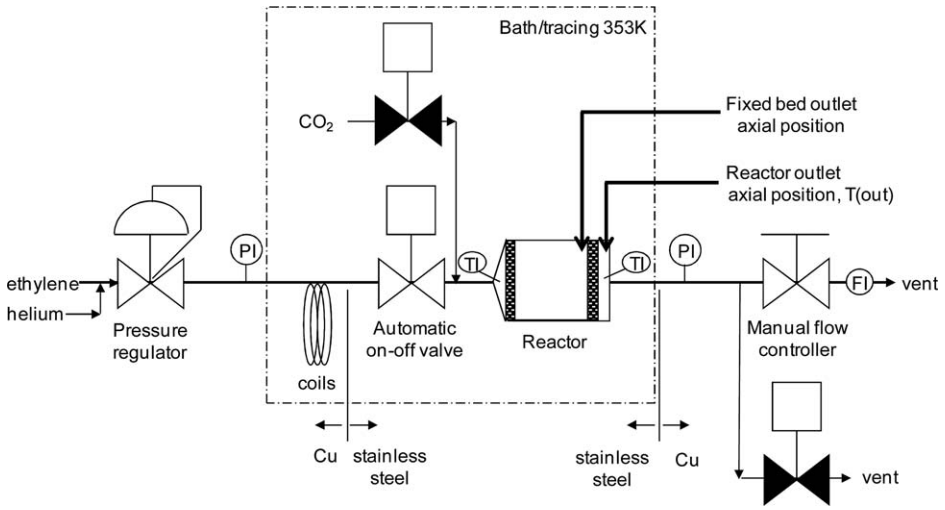

Figure 1. Process flow diagram of the reactor system.

the fixed bed and found to be non-negligible. The model type is, therefore, bidimensional and heterogeneous with two separate phases taken into account: (1) the gas and inert solid and (2) the catalyst and polymer. Mass transfer limitations within the catalyst/polymer particle may also be possible and are lumped into a simple parameter which represents the overall reaction kinetics to be estimated in this work by the observer.

The data and correlations required to represent the fluid physical properties are drawn from the literature.[19,20] Ethylene concentration is assumed to be at equilibrium between the gas and polymer phase and is described using Henry's Law. Heat-transfer coefficients and effective conductivities are determined according to accepted correlations for fixed beds.[21–25] The temperatures are measured in the reactor inlet and outlet chambers and the hot water bath external to the stainless steel reactor wall. The wall and the frits which support the reactor bed are relatively thick. So the heat capacity of these elements cannot be neglected and they are included in the reactor model. However, as will be seen later, the frit and the wall are not included in the observer since there is no reaction taking place there. So the observer may use a calculated reactor bed outlet temperature, upstream of the exit frit.

Plug flow and constant hot water bath temperature are assumed. The pressurization time of the reactor was measured and found to reach full pressure after approximately 1 s, following the behavior of a first order system. This is of the same order as the shortest experiments and total pressure is, therefore, included as a variable in the reactor model. During pressurization, the reactor exit gas flow rate is kept directly proportional to the reactor pressure. It is assumed that once the reactor pressure is stable the reaction gas exit flow rate is constant and consumption of ethylene in the reactor is compensated by increased flow of incoming reaction gas. For a full discussion of these points refer to the earlier work.[6]

The material balances given in Eqs. 1 and 2 are used to represent the gas phase mole fraction of ethylene and the mass of accumulating polymer, respectively. The reaction gas flow rate decreases along the length of the reactor as ethylene is consumed, Eq. 3

$$\frac{\partial y_{C2}}{\partial t}=\frac{-1}{\left(\frac{P\varepsilon}{RT_g}\right)}\left(r_v(1+y_{C2})-F_T\frac{\partial y_{C2}}{S_r\partial z}\right.$$
$$\left.-\frac{D_r\varepsilon P}{rRT_g}\frac{\partial}{\partial r}\left(r\frac{\partial y_{C2}}{\partial r}+\frac{y_{C2}}{T_g}\frac{\partial T_g}{\partial r}\right)+\left(\frac{y_{C2}\varepsilon P}{RT_g^2}\right)\frac{\partial T_g}{\partial t}\right) \quad (1)$$

$$\frac{dM_R}{dt}=Mwt_{C2}r_v \quad (2)$$

$$\frac{dF_T}{S_r dz}=-r_v \quad (3)$$

where r_v represents the overall reaction rate to be estimated in this work using an observer. The boundary conditions, given by Eqs. 4–9, are: constant ethylene inlet concentration, zero ethylene concentration in the reactor wall, no change of ethylene concentration in the inlet and outlet frits, ethylene concentration symmetrical about the reactor center line and no mass transfer of ethylene into the reactor wall

$$y_{C2}=y_{C20}|_{z=0}\forall r \quad (4)$$

$$y_{C2}=0|_{d_{reac}/4<r<d_{reac}/2}\forall z \quad (5)$$

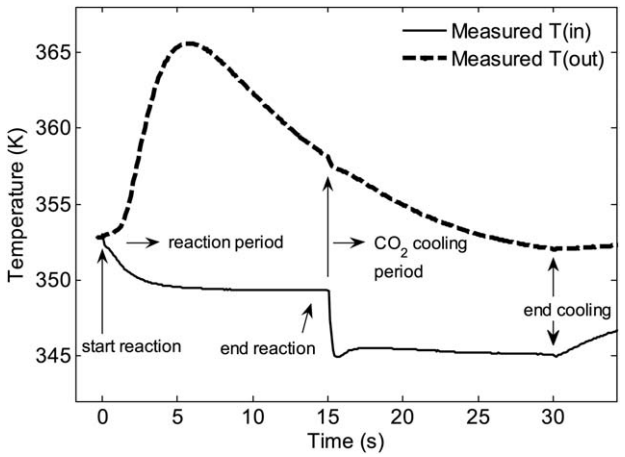

Figure 2. Temperature measurements for typical reaction of duration 15 s.

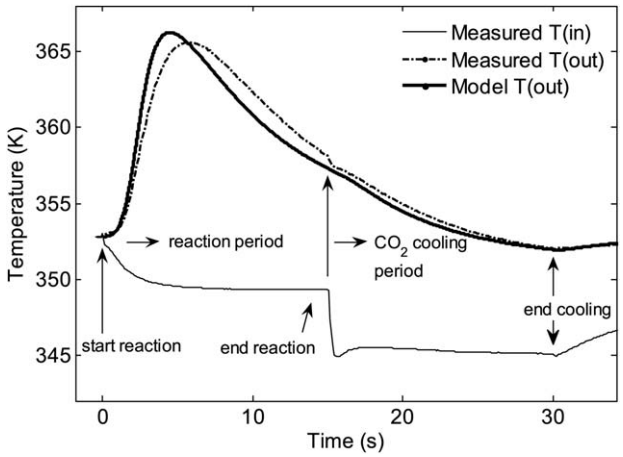

Figure 3. Comparison of calculated output temperatures against measured values for an experiment of 15 s duration ($T = 353$ K, $P = 6.67.105$ N m^{-2} of C_2H_4, nominal gas/particle velocity = 0.11 m/s).

$$\left.\frac{\partial y_{C2}}{\partial z}=0\right|_{\substack{0<z<lf1\\(lr-lf2)<z<l_{reac}}} \tag{6}$$

$$\left.\frac{\partial y_{C2}}{\partial r}=0\right|_{r=0} \tag{7}$$

$$\left.\frac{\partial y_{C2}}{\partial r}=0\right|_{r=d_{reac}/4} \tag{8}$$

The heat balances for the catalyst/polymer phase in the reactor and for the gas/inert phase are given by Eqs. 9 and 10 respectively

$$\frac{dT_C}{dt}=\frac{1}{\sum\left(\rho c_p\right)_c}\left(\mathrm{Mwt}_{C2}r_v\left(\frac{\Delta H}{\mathrm{Mwt}_{C2}}+c_{pC2}\left(T_g-T_c\right)\right)+S_{cat}h_{cat}\left(T_g-T_c\right)\right) \tag{9}$$

$$\frac{\partial T_g}{\partial t}=\frac{1}{\sum\left(\rho c_p\right)_g}\left(-\left(S_{cat}h_{cat}-\mathrm{Mwt}_{C2}r_vc_{pC2}\right)\left(T_g-T_c\right)+F_T\mathrm{Mwt}_{rg}c_{prg}\frac{\partial T_g}{S_r\partial z}+\frac{l_{sfer}}{r}\frac{\partial}{\partial r}\left(\frac{r\partial T_g}{\partial r}\right)\right) \tag{10}$$

The boundary conditions for the heat balances (given by Eqs. 11–14) are: use conductivity of stainless steel for the reactor wall; reactor bed temperature symmetrical about the centerline; heat transfer rates from fixed bed to reactor wall and from reactor wall to hot water bath both determined from the respective heat-transfer coefficients.

$$l_{sfer}=\left.l_{s\_inox}\right|_{d_{reac}/4<r<d_{reac}/2}\forall z \tag{11}$$

$$\left.\frac{\partial T_g}{\partial r}=0\right|_{r=0}\forall z \tag{12}$$

$$l_{sfer}\left(\frac{\partial T_g}{\partial r}\right)=\left.h_{int}^{sf}\left(T_g-T_w\right)\right|_{r=d_{reac}/4}\forall z \tag{13}$$

$$l_{s\_inox}\left(\frac{\partial T_g}{\partial r}\right)=\left.h_{bath}\left(T_w-T_b\right)\right|_{r=d_{reac}/2}\forall z \tag{14}$$

Model simulation

The objective of this work is to estimate the polymerization rate, which is difficult to model during the first stage of the polymerization due to rapid and significant changes in particle morphology, physical properties, and mass transfer rates. Moreover, the observer should not only be applicable to the current catalyst type and support but also suitable for testing potential alternatives. To validate the observer first by simulation, an empirical relation is used to represent the reaction rate, based on experimental observations. Further validation of the observer is then done using the experimental data.

For simplicity, the kinetics are described by Eq. 15 as a single reaction with a lumped reaction parameter, $k_{p0}C^*$, which represents all the effects impacting the reaction rate. This is an empirical parameter, specific to our reactor and data, and includes, for example, the efficiency of the catalyst particle. The experimental data shows that the overall polymerization rate tends to decrease rapidly during the first moments of the polymerization. To follow the overall reaction rate as closely as possible, the value of $k_{p0}C^*$ is reduced as the polymerization progresses and adjusted by optimization to get the best fit between measured and calculated output temperatures. The form used is given in Eq. 17.

$$r_v=k_{p0}C^*e^{-\frac{Ea_p}{RT}}C_{C2} \tag{15}$$

where,

$$C_{C2}=y_{C2}\mathrm{PH}(T) \tag{16}$$

and

$$k_{p0}C^*=a-b(M_R)^c \tag{17}$$

The PDEs representing the heat and mass balances were discretized using the finite element method. The ODEs obtained and the lumped reaction constant and the reactor pressure are all integrated in MATLAB using the default solver, ode45, which was found to be sufficient when compared to the other solvers available.

The model was simulated using real inputs. The reaction gas flow rate, physical properties and heat transfer correlations that were all set to correspond to the initial conditions and then updated every 0.02 s. For observer development, it was chosen to work with an experiment of 15 s to remain within the duration of interest, while minimising the impact of the reactor pressurization dynamic and the fraction of heat generated by the polymerization which exits the reactor during the cooling period.

Figures 3–5 give simulation results relating to the same experiment of 15 s duration with 46.2 mg of catalyst and a calculated mass of polymer formed of 37.1 mg for 33.3 mg measured. Figure 3 shows the fit between calculated and measured reactor outlet temperatures. Figures 4a, b show calculated temperatures for the reactor bed and catalyst/polymer. The values are significantly higher than those measured at the reactor outlet, with a steep gradient predicted along the reactor length and a brief temperature excursion above the polymer melting point after around 1.6 s of reaction. This is followed by a rapid reduction in the bed temperature as the polymerization rate decreases. The calculated temperatures for the catalyst/polymer are very similar to those found for the gas/inert for these experimental conditions. Figure 5 gives the maximum radial temperature profile for the reactor bed at the hot spot, with a fairly flat profile across the center of the bed, a cool section close to the reactor wall and only a slight gradient within the reactor wall. These simulation results will be useful to establish some model simplifications.

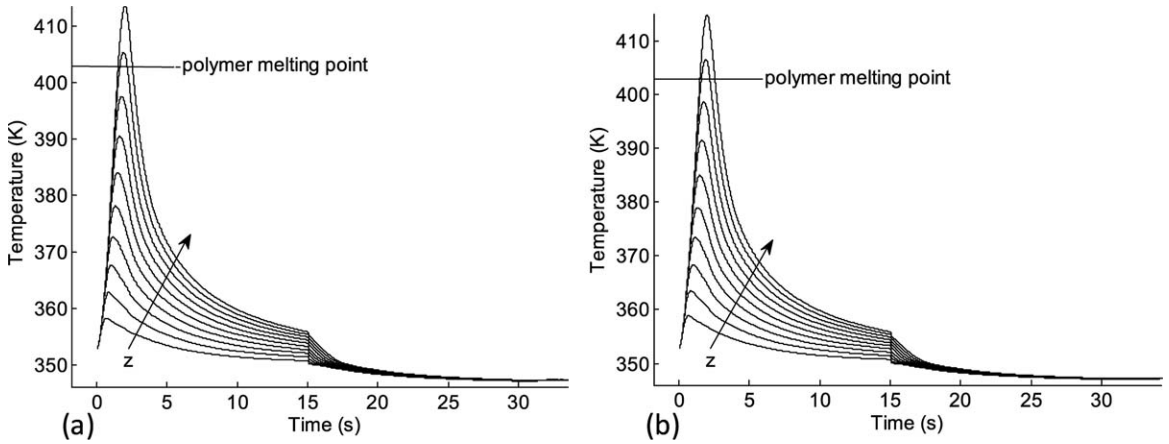

Figure 4. Calculated temperatures at fixed 1 mm intervals along the length of the reactor bed (a) gas and inert solid and (b) catalyst/polymer.

High Gain Observers

Theoretical background

Different observer methodologies have been applied to estimate the reaction rate in homogeneous chemical reactors described by ODEs, such as Kalman filters,[26] high gain observers for copolymerization reactions[27] and receding horizon observers for a terpolymerization reaction.[28] As the stop flow reactor model is discretized to give a set of ODEs, such observers can also be considered here. In this work, a simple form of high gain observer[29,30] is used to estimate the reaction rate.

Consider the following nonlinear system:

$$\begin{aligned} \dot{x}(t) &= f(x(t), u(t)) \\ y(t) &= h(x(t)) \end{aligned} \tag{18}$$

where $x(t) \in M$, $M \in \Re^n$ is the state space, $y \in \Re$ the measured outputs and $u \in U$, $U \in \Re^m$ is the bounded input space. f is C^∞ vector fields on $\Re^n$ and h, a C^∞ scalar field on $\Re^n$.

Definition 1. *The function f is global Lipschitz if* $\exists\ c > 0$ *such that* $\forall\ x, x' \in R^n$

$$|f(x) - f(x')| \leq c\|x - x'\| \tag{19}$$

The following assumptions are needed in the sequence:

H1) *The system (18) is locally uniformly observable, that is, observable* $\forall$ *input.*

H2) **Theorem 1.**[29,30] *If the system is uniformly observable, the change of coordinates,* $\phi(x)$*, for the system (18) given by*

$$\xi = \phi(x) = \begin{bmatrix} h(x) \\ L_f h(x) \\ \vdots \\ L_f^{n-1} h(x) \end{bmatrix} \tag{20}$$

which is a global diffeomorphism with respect to x leads to the following system

$$\begin{cases} \dot{\xi}(t) = A\xi(t) + F(\xi(t)) + \sum_{i=1}^{m} u_i(t) g_i(\xi(t)) \\ y(t) = C\xi(t) \end{cases} \tag{21}$$

with

$$A = \begin{pmatrix} 0 & 1 & 0 & \dots & 0 \\ 0 & 0 & 1 & & \vdots \\ \vdots & & & \ddots & 0 \\ 0 & & & & 1 \\ 0 & \dots & & 0 & 0 \end{pmatrix}, F(\xi) = \begin{pmatrix} 0 \\ \vdots \\ 0 \\ F_n(\xi) \end{pmatrix}, C = [1 \quad 0 \quad \dots \quad 0] \text{ and}$$

$$\begin{cases} g_j(\xi) = [g_{j1}(\xi) \quad \cdots \quad g_{jn}(\xi)]^T \\ g_{ji}(\xi) = g_{ji}(\xi_1, ..., \xi_i) \end{cases}, 1 \leq i \leq n \text{ and } 1 \leq j \leq m \tag{22}$$

where $L_f y$ *is the Lie derivative of the function f in the direction of y.*

H3) *The nonlinear terms F,* g_1*, ., *g_m *are global Lipschitz. This assumption is always reliable if the states are bounded.*

Theorem 2.[30] *For* $\theta > 0$ *and sufficiently large, the system*

$$\dot{\hat{\xi}}(t) = A\hat{\xi} + F\left(\hat{\xi}(t)\right) + \sum_{i=1}^{m} u_i(t) g_i\left(\hat{\xi}(t)\right) - S_\theta^{-1} C^T \left(C\hat{\xi}(t) - y(t)\right) \tag{23}$$

is an exponential observer of the state ξ *of the system (18) and* S_θ *is the unique symmetric positive definite matrix satisfying the algebraic Lyapunov equation*

$$\theta S_\theta + A^T S_\theta + S_\theta A - C^T C = 0 \tag{24}$$

which gives

$$S_\theta(i,j) = \frac{(-1)^{i+j}}{\theta^{i+j-1}} \frac{(i+j-2)!}{(i-1)!(j-1)!} \tag{25}$$

The observer for the original state x(t) in system (18) is given by

$$\dot{\hat{x}}(t) = f(\hat{x}(t), u) - \left(\frac{\partial \phi}{\partial x}\Big|_{\hat{x}(t)}\right)^{-1} S_\theta^{-1} C^T (C\hat{x}(t) - y(t)) \tag{26}$$

$\hat{x}$ is the estimated values of x.

The gain used does not require the resolution of any dynamical system and it is explicitly given. The tuning of the estimator is reduced to the calibration of a single parameter. Moreover, the observer can provide estimates of some parameters from only their effect, and therefore, without requiring a model for them.

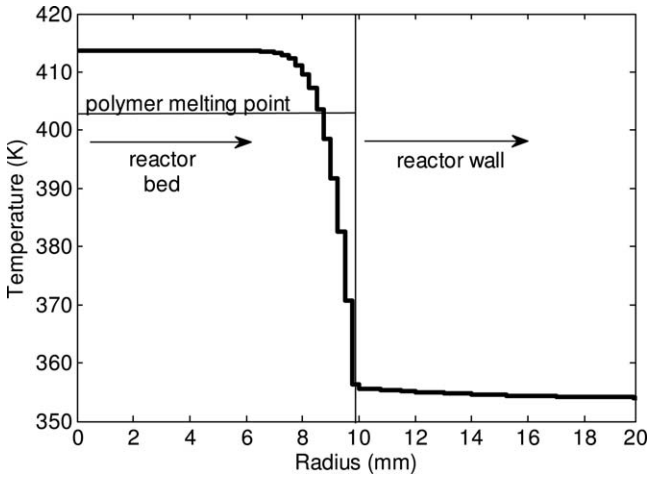

Figure 5. Calculated radial bed (gas/inert) temperature profiles in final axial element of reactor bed (hot spot).

Observer implementation

Based on the simulation results, some model simplifications are made in view of the observer development. First, note that only the heat balances Eqs. 9 and 10 are required, as it is these which relate the reaction rate to the outlet temperature. In these balances, the term $c_{pC2}(T_g - T_c)$ represents catalyst particle cooling by incoming ethylene which is small compared to the heat of reaction and can be neglected. The heat balances become

$$\frac{\partial T_c}{\partial t} = \frac{1}{\sum (\rho c_p)_c}\left(\Delta H r_v + S_{cat} h_{cat}\left(T_g - T_c\right)\right) \tag{27}$$

and

$$\frac{\partial T_g}{\partial t} = \frac{1}{\sum (\rho c_p)_g}\left(-S_{cat} h_{cat}\left(T_g - T_c\right) + F_T \mathrm{Mwt}_{rg} c_{prg} \frac{\partial T_g}{S_r \partial z} + \frac{l_{sfer}}{r}\frac{\partial}{\partial r}\left(\frac{r \partial T_g}{\partial r}\right)\right) \tag{28}$$

Second, the position at which the reactor outlet temperature is measured (see Figure 1) is not the measured output used by the observer. The reactor model includes the reactor wall and frits, where there is heat transfer but no reaction

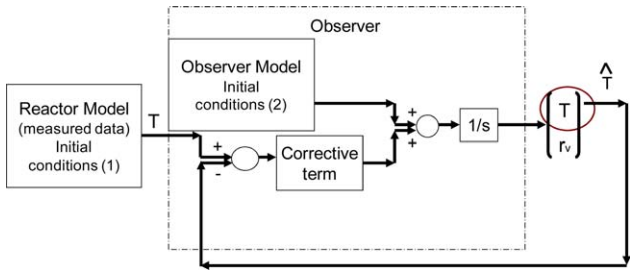

Figure 6. Block diagram of the observer. [Color figure can be viewed in the online issue, which is available at wileyonlinelibrary.com.]

takes place. As the reaction rate in these volumes is known to be zero, there is no need to run the observer there. However, the observer does require the fixed bed outlet temperature which is not physically measured. It is assumed that the heat transfer calculations for these parts of the reactor are correct and the fixed bed outlet temperature, calculated by the model is the value taken by the observer as the measured variable.

Third, all the parameters in the heat balances except T_c, T_g, and r_v are assumed constant. This includes T_w, F_T, and ρc_p. Note that for the model these parameters were considered as variables. However, the experiments chosen for observer development are at maximum flow rate through the reactor bed and the change in flow rate along the reactor length is, therefore, minimized. Also, the previous simulations showed that wall temperature variation is slight and with the reactor bed considered as homogeneous the accumulation of polymer makes little difference to the overall heat capacity of the bed.

Fourth, thermal gradients are known to exist in the reactor bed. In the reactor model, these are accounted for by using finite elements in both the radial and axial directions. In this work, we will construct observers

1. By including only finite elements in the axial direction (1-D observer).
2. By including both axial and radial temperature gradients (2-D observer).

For the 1-D observer, a different wall heat-transfer coefficient is used. The resistance to heat transfer in the reactor bed and at the wall are combined in an overall heat-transfer coefficient, as determined from Eq. 29[31]

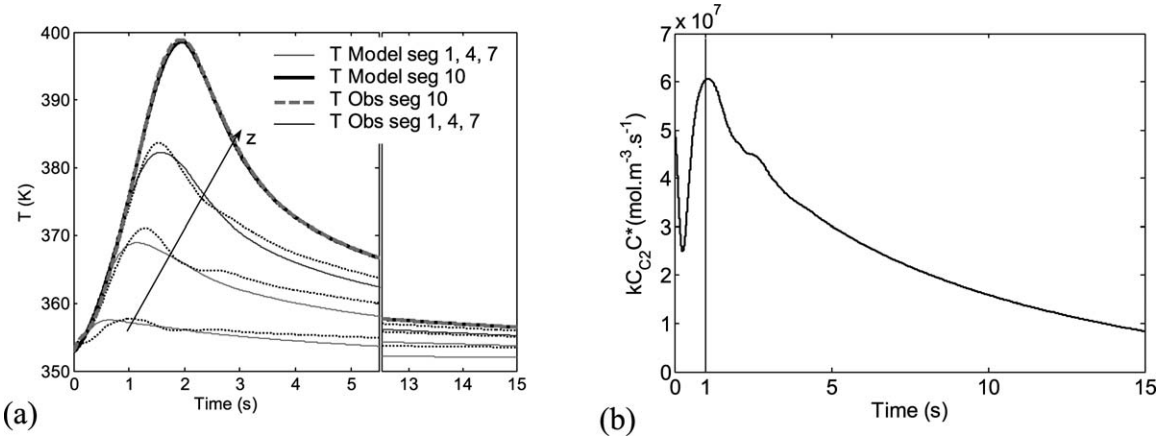

Figure 7. Results of the 1-D observer for $k_{p0}C_{C2}C^*$ with 10 axial reactor elements (a) Comparison of T to bed temperatures calculated by the model and (b) $k_{p0}C_{C2}C^*$.

$$\frac{1}{\bar{h}_{\text{int}}} = \frac{d_t}{8 l_{\text{sfer}}} + \frac{1}{h_{\text{int}}^{\text{sf}}} \tag{29}$$

To construct an observer, Eqs. 27 and 28 must be discretized and written in state space form. The method is the same for both the 1-D and 2-D observers, but the representation for the 1-D observer is simpler and shown here for the sake of brevity. So, after discretization into n axial elements, i, the heat balance for the gas/inert phase can be written

$$\frac{dT_{gi}}{dt} = \frac{1}{\sum (\rho c_{\text{p}})_g} \left(-S_{\text{cat}} h_{\text{cat}} (T_{gi} - T_{ci}) + F_T \text{Mwt}_{\text{rg}} c_{\text{prg}} \frac{(T_{gi} - T_{g_{i-1}})}{S_{\text{r}} dz} - \bar{h}_{\text{int}} A_w (T_{gi} - T_{\text{w}}) \right) \tag{30}$$

The state-space form of the 1-D model for each individual element is therefore

$$\underbrace{\begin{bmatrix} \dot{T}_{gi} \\ \dot{T}_{ci} \\ \dot{r}_{vi} \end{bmatrix}}_{\dot{X}} = \underbrace{\begin{bmatrix} \frac{1}{\sum (\rho c_{\text{p}})_g} \left(-S_c h_{\text{cat}} + \frac{F_{\text{T}} \text{Mwt}_{\text{rg}} c_{\text{prg}}}{S_{\text{r}} dz} + \bar{h}_{\text{int}} A_{\text{w}} \right) & \frac{S_c h_{\text{cat}}}{\sum (\rho c_p)_g} & 0 \\ \frac{S_{\text{c}} h_{\text{cat}}}{\sum (\rho c_p)_c} & \frac{-S_c h_{\text{cat}}}{\sum (\rho c_{\text{p}})_c} & \frac{\Delta H}{\sum (\rho c_{\text{p}})_c} \\ 0 & 0 & 0 \end{bmatrix}}_{A} \cdot \underbrace{\begin{bmatrix} T_{gi} \\ T_{ci} \\ r_{vi} \end{bmatrix}}_{X} + \underbrace{\begin{bmatrix} \frac{1}{\sum (\rho c_{\text{p}})_g} \left(-F_{\text{T}} \text{Mwt}_{\text{rg}} c_{\text{prg}} \frac{T_{g_{i-1}}}{S_{\text{r}} dz} - \bar{h}_{\text{int}} A_{\text{w}} T_{\text{w}} \right) \\ 0 \\ \varepsilon \end{bmatrix}}_{\varphi} \tag{31}$$

where ε represents the unknown dynamic of r_{v} (t). Note that A depends only on measured or known variables and the other terms are in ϕ.

Finally, at the particular experimental conditions considered, the reactor model predicts very similar values for T_{g} and T_{c}. These can, therefore, be combined into a single variable, T, for the purpose of observer development in this case. Note that for different reaction conditions, for example, alternative flow rates or catalyst particle sizes, this simplification might not be valid and in that case the observer should be constructed based on Eq. 31.

The heat balance over a finite element for the 1-D observer becomes

$$\frac{dT_i}{dt} = \frac{1}{\sum \rho c_{\text{p}}} \left(\Delta H r_{vi} + F_{\text{T}} \text{Mwt}_{\text{rg}} c_{\text{prg}} \frac{(T_i - T_{i-1})}{S_{\text{r}} dz} - \bar{h}_{\text{int}} A_{\text{w}} (T_i - T_{\text{w}}) \right) \tag{32}$$

And the state-space form of the augmented system (considering r_{vi} as a state) becomes

$$\underbrace{\begin{bmatrix} \dot{T}_i \\ \dot{r}_{vi} \end{bmatrix}}_{\dot{X}} = \underbrace{\begin{bmatrix} \frac{1}{\sum \rho c_{\text{p}}} \left(\frac{F_{\text{T}} \text{Mwt}_{\text{rg}} c_{\text{prg}}}{S_{\text{r}} dz} + \bar{h}_{\text{int}} A_{\text{w}} \right) & \frac{\Delta H}{\sum \rho c_{\text{p}}} \\ 0 & 0 \quad 0 \end{bmatrix}}_{A} \cdot \underbrace{\begin{bmatrix} T_i \\ r_{vi} \end{bmatrix}}_{X} + \underbrace{\begin{bmatrix} \frac{1}{\sum \rho c_{\text{p}}} \left(-F_{\text{T}} \text{Mwt}_{\text{rg}} c_{\text{prg}} \frac{T_{i-1}}{S_{\text{r}} dz} - \bar{h}_{\text{int}} A_{\text{w}} T_{\text{w}} \right) \\ \varepsilon \end{bmatrix}}_{\varphi} \tag{33}$$

To usefully apply a state observer to a system of equations, they must be observable. This requires that the state(s) to be estimated can be completely defined over the required time interval from knowledge of the inputs and measured outputs. The Kalman criterion can be used to test the observability of a linear system of equations. This criterion shows that our system is observable for a single reactor element (assuming no radial and axial gradients), but this cannot be confirmed for multiple elements Eq. 31. Note that assuming a single element means there are no temperature gradients in the reactor, which is of course not the case, as demonstrated by the model simulations.

Figure 6 shows a block diagram of the observer implementation with the reactor as a single element. As expected, if we develop an observer for a single element model, poor estimates of the reaction rate are obtained. Indeed, the reactor bed outlet temperature used as the observer input corresponds to a reactor hot spot, with lower

temperatures and reaction rates throughout the rest of the bed. The result is an overestimate of the reaction rate and mass of polymer by the observer with 87.6 mg estimated for 33.3 mg measured.

Discretising in the axial and radial directions gives a specific number of finite reactor elements on which the observer can be applied similarly. However, it was confirmed that this discretized representation of the reactor bed was not observable for multiple elements.

So, the single element observer is not appropriate for the present reactor and the reaction rate becomes unobservable if we consider multiple elements. To create an observer that takes into account the axial thermal gradient in the reactor bed using finite elements, an observable system of equations is required. In general, reaction rates vary with temperature according to their activation energy and an accepted form of the reaction rate equation for ethylene polymerization was given previously in Eq. 15

$$r_v = k_{p0} C^* e^{-\frac{Ea_p}{RT}} C_{C2}$$

Considering the impact of the individual terms in this equation; the activation energy increases the reaction rate by a factor of at least 4 between the reactor inlet and outlet, the concentration of ethylene in the reactor bed is calculated to vary by less than 5% and the variation in the active site concentration during the experiments is not known. However, the catalyst distribution is initially uniform, as the bed is well mixed during preparation. Based on this, if it is assumed that all the variation in polymerization rate in the reactor bed at any one moment is due to the activation energy of the propagation reaction, it is no longer necessary to estimate a reaction rate for each individual reactor element. Instead, an observer for a single variable, $K = k_{p0} C_{C2} C^*$, can be created. From the point of view of the observer, this system is much simpler to estimate since there are now fewer unknown variables; the temperature in each element and a single reaction rate parameter. The previous system required as many reaction rate values to be estimated as there were finite elements. Note that a 2-D simulation is still required even though only a single parameter is to be estimated.

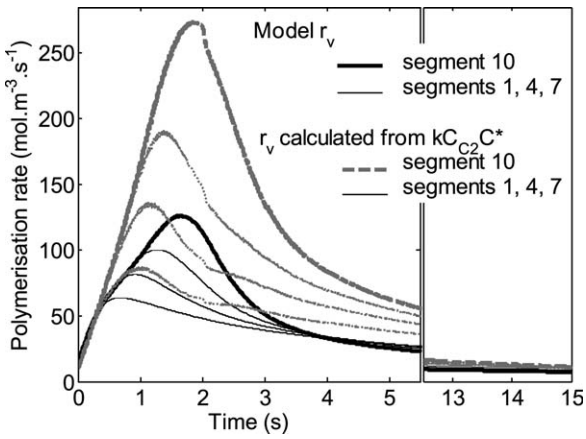

Figure 8. Comparison of polymerization rate calculated using model and from the 1-D observer for $k_{p0}C_{C2}C^*$ with 10 axial reactor elements.

In the following, we consider the estimation of K, from which the reaction rate can be calculated. The simplified model presented in Eq. 32 is combined with Eq. 15

$$\frac{dT_i}{dt} = \frac{1}{\sum \rho c_p} \left(\Delta H K e^{-\frac{Ea_p}{RT_i}} + F_T \mathrm{Mwt_g} c_{prg} \frac{(T_i - T_{i-1})}{S_r dz} - \bar{h}_{int} A_w (T_i - T_w) \right) \tag{34}$$

1-D observer for K (axial discretization)

The observer will have two states T and K. First, only axial discretization is considered (assuming no radial gradients), with n finite reactor elements:

Let $\dot{K} = 0$

Write the equations in matrix form

$$\underbrace{\begin{bmatrix} \dot{T}_n \\ \vdots \\ \dot{T}_2 \\ \dot{T}_1 \\ \dot{K} \end{bmatrix}}_{\dot{X}} = \underbrace{\begin{bmatrix} \frac{1}{\sum (\rho c_p)} \left(K e^{\frac{-E_a}{RT_n}} \Delta H + F_{in} \mathrm{Mwt_g} c p_g \frac{T_n - T_{n-1}}{S_r dz} - \bar{h}_{int} A_w T_n \right) \\ \vdots \\ \frac{1}{\sum (\rho c_p)} \left(K e^{\frac{-E_a}{RT_2}} \Delta H + F_{in} \mathrm{Mwt_g} c p_g \frac{T_2 - T_1}{S_r dz} - \bar{h}_{int} A_w T_2 \right) \\ \frac{1}{\sum (\rho c_p)} \left(K e^{\frac{-E_a}{RT_1}} \Delta H + F_{in} \mathrm{Mwt_g} c p_g \frac{T_1 - T_{in}}{S_r dz} - \bar{h}_{int} A_w T_1 \right) \\ 0 \end{bmatrix}}_{f(x)} + \underbrace{\begin{bmatrix} \frac{\bar{h}_{int} A_w T_w}{\sum (\rho c_p)} \\ \vdots \\ \frac{\bar{h}_{int} A_w T_w}{\sum (\rho c_p)} \\ \frac{\bar{h}_{int} A_w T_w}{\sum (\rho c_p)} \\ \varepsilon \end{bmatrix}}_{\varphi} \tag{35}$$

Note that the system is nonlinear so we can no longer write the matrix A and the observer correction term will be time-dependent. In this arrangement, the state vector, X, is written with the measured bed temperature at reactor element n in row 1. This is necessary for the observer design.

As aforementioned, a number of observers could be applied to this system. To apply the observer defined in Eq. 23, we carry out a change of variables as follows to get a canonical form of observability

$$Z=\begin{bmatrix} z_1 \\ z_2 \end{bmatrix}=\begin{bmatrix} y \\ L_f y \end{bmatrix}=\begin{bmatrix} y \\ \dfrac{dy}{dX}f \end{bmatrix} \tag{36}$$

Applying this to any element of the reactor gives

$$z_1=y=T \tag{37}$$

$$z_2=\frac{dy}{dX}f=\left[\frac{dT}{dT}f_1+\frac{dT}{dK}f_2\right]=[1.f_1+0]$$
$$=\frac{1}{\sum(\rho c_{\mathrm{p}})}\left(Ke^{\frac{-E_a}{RT}}\Delta H+F_{in}\mathrm{Mwt_g}cp_{\mathrm{g}}\frac{dT}{S_{\mathrm{r}}dz}-\bar{h}_{\mathrm{int}}A_{\mathrm{w}}T\right) \tag{38}$$

And so

$$\frac{dz}{dX}=\begin{bmatrix} 1 & 0 \\ \dfrac{-1}{\sum(\rho c_{\mathrm{p}})}\left(\dfrac{E_{\mathrm{a}}}{RT^2}Ke^{\frac{-E_{\mathrm{a}}}{RT}}\Delta H+\dfrac{F_{in}\mathrm{Mwt_g}cp_{\mathrm{g}}}{S_{\mathrm{r}}dz}+h_{\mathrm{int}}^{\mathrm{sf}}A_{\mathrm{w}}\right) & \dfrac{\Delta He^{\frac{-E_a}{RT}}}{\sum(\rho c_{\mathrm{p}})} \end{bmatrix} \tag{39}$$

Finally, the observer correction term can be written and combined with the model described by Eq. 35, to get the form given in Eq. 26. Note that Eq. 39, and hence the correction term of the observer, is time variable.

To check the results of the 1-D observer, comparison was made against the reactor model outputs. To do this, the average temperatures and reaction rates over the radial elements of each axial segment were calculated from the model outputs, taking account of the variation in segment volume across the reactor radius. Figure 7 shows the result of applying this observer to the reactor bed divided into 10 discrete elements. Temperatures determined from the reactor model and the observer are reported in Figure 7a for four axial reactor elements, with those from the model serving as expected values. The temperature decay is smooth in the interval between the times reported in the figure. The observer recalculates the measured temperature correctly and predicts values for the other elements which are consistent with those of the model. Figure 7b gives the estimated profile for $k_{\mathrm{p0}}C_{\mathrm{C2}}C^*$. In this simulation, the observer is initialized close to the initial value of the model. A convergence period can be observed in the first part of the graph. The observer gets far from the model then reaches a minimum as it moves closer to the model until complete convergence. The estimation error is accumulated during this convergence period and is used to allow the observer to correct modelling errors and move to useful predictions of $k_{\mathrm{p0}}C_{\mathrm{C2}}C^*$.

Figure 8 shows the reaction rates found in segments 1, 4, 7, and 10, based on the estimation of $k_{\mathrm{p0}}C_{\mathrm{C2}}C^*$. These are still above those of the model and the calculated total mass of polymer for this case is 62.9 mg, which is closer to the measured value of 33.3 mg (compared to a single element observer), but still too high.

It seems that the observer is over estimating the heat transfer rate at the reactor wall. To match the total mass of polymer to the measured value, the heat-transfer coefficient used in the observer must be reduced by a factor of 10. As the observer is only discretized in 1-D, while the model is 2-D, the observer makes the big assumption that each element is homogeneous in temperature while only part of the volume is touching the wall. An empirical apparent heat-transfer coefficient can be estimated to force the observer to return the real polymer mass, but the best way to account for this heterogeneity would be to develop a 2-D observer. Indeed, in discussing the correlation for the wall heat-transfer coefficient given in Eq. 29, Froment[31] states that "except for 'mild' conditions, the 1-D model may fail to predict the mean temperatures." Also the correlation was derived for beds of porosity close to 0.4, formed of spherical particles and with Reynolds number >3, which is not our case. The next step in observer development is, therefore, to eliminate this correlation by creating a 2-D observer for the reactor bed, accounting for the effective conductivity in the bed and the wall heat-transfer coefficient separately.

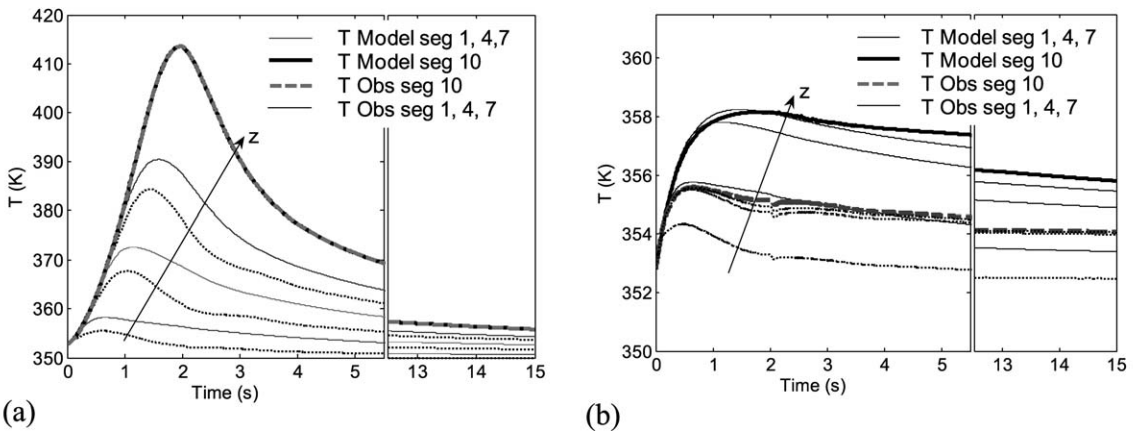

Figure 9. Results of the 2-D observer for $k_{\mathrm{p0}}C_{\mathrm{C2}}C^*$ with 10 axial and 5 radial bed elements.

Comparison of T to bed temperatures calculated by the model (a) center and (b) edge.

2-D observer for K (axial and radial discretization)

For the 2-D observer both axial and radial discretization are considered, with n finite reactor elements, i, in the axial direction, and m finite reactor elements, j, in the axial direction. The reactor model becomes

$$\frac{\partial T}{\partial t}=\frac{1}{\sum \rho c_{\mathrm{p}}}\left(\Delta HKe^{-\frac{Ea_{\mathrm{p}}}{\mathrm{RT}}}+F_{\mathrm{T}}\mathrm{Mwt}_{\mathrm{rg}}c_{\mathrm{prg}}\frac{\partial T}{S_{\mathrm{r}}\partial z}+\frac{l_{\mathrm{sfer}}}{r}\frac{\partial}{\partial r}\left(\frac{r\partial T}{\partial r}\right)\right) \tag{40}$$

$$\frac{\partial T}{\partial r}=0|_{r=0}\forall z \tag{41}$$

$$l_{\mathrm{sfer}}\left(\frac{\partial T}{\partial r}\right)=h_{\mathrm{int}}^{\mathrm{sf}}(T-T_{\mathrm{w}})|_{r=d_{\mathrm{reac}}/4}\forall z \tag{42}$$

Following the same methodology as for the 1-D observer, this reactor model is discretized into finite elements

$$\frac{dT_{i,j}}{dt}=\frac{1}{\sum \rho c_{\mathrm{p}}}\left(\Delta HKe^{-\frac{Ea_{\mathrm{p}}}{\mathrm{RT}_{i,j}}}+F_{\mathrm{T}}\mathrm{Mwt}_{\mathrm{rg}}c_{\mathrm{prg}}\frac{\left(T_{i,j}-T_{i-1,j}\right)}{S_{\mathrm{r}}\partial z}+\frac{l_{\mathrm{sfer}}\left(T_{i,j-1}-2T_{i,j}+T_{i,j+1}\right)}{dr^2}\right) \tag{43}$$

The progrmmed boundary conditions are

$$T_{i,j-1}=T_{i,j}|_{j=1}\forall z$$
$$\frac{l_{\mathrm{sfer}}\left(-T_{i,j}+T_{i,j+1}\right)}{dr^2}=h_{\mathrm{int}}^{\mathrm{sf}}\left(T_{i,j}-T_{w}\right)|_{j=m}\forall z \tag{44}$$

Writing these equations in state space form

$$\begin{bmatrix}\dot{T}_{n,1}\\ \dot{T}_{n,2}\\ \vdots\\ \dot{T}_{n,m}\\ \vdots\\ \vdots\\ \dot{T}_{1,m-1}\\ \dot{T}_{1,m}\\ \dot{K}\end{bmatrix}=\underbrace{\begin{bmatrix}\frac{1}{\sum \rho c_{\mathrm{p}}}\left(\Delta HKe^{-\frac{Ea_p}{\mathrm{RT}n,1}}+F_T Mwt_{rg}c_{prg}\frac{\left(T_{n,1}-T_{n-1,1}\right)}{S_r\partial z}+\frac{l_{sfer}\left(-T_{n,1}+T_{n,2}\right)}{dr^2}\right)\\ \frac{1}{\sum \rho c_{\mathrm{p}}}\left(\Delta HKe^{-\frac{Ea_p}{\mathrm{RT}n,2}}+F_{\mathrm{T}}\mathrm{Mwt}_{\mathrm{rg}}c_{\mathrm{prg}}\frac{\left(T_{n,2}-T_{n-1,2}\right)}{S_{\mathrm{r}}\partial z}+\frac{l_{\mathrm{sfer}}\left(T_{n,1}-2T_{n,2}+T_{n,3}\right)}{dr^2}\right)\\ \vdots\\ \frac{1}{\sum \rho c_{\mathrm{p}}}\left(\Delta HKe^{-\frac{Ea_p}{\mathrm{RT}n,m}}+F_{\mathrm{T}}\mathrm{Mwt}_{\mathrm{rg}}c_{\mathrm{prg}}\frac{\left(T_{n,m}-T_{n-1,m}\right)}{S_r\partial z}+\frac{l_{\mathrm{sfer}}\left(T_{n,m-1}-T_{n,m}\right)}{dr^2}-h_{\mathrm{int}}^{sf}A_{\mathrm{w}}T_{m,n}\right)\\ \vdots\\ \vdots\\ \frac{1}{\sum \rho c_{\mathrm{p}}}\left(\Delta HKe^{-\frac{Ea_p}{\mathrm{RT}i,j}}+F_{\mathrm{T}}\mathrm{Mwt}_{\mathrm{rg}}c_{\mathrm{prg}}\frac{\left(T_{1,m}-T_{in,m}\right)}{S_r\partial z}+\frac{l_{\mathrm{sfer}}\left(T_{1,m-2}-2T_{1,m-1}+T_{1,m}\right)}{dr^2}\right)\\ \frac{1}{\sum \rho c_{\mathrm{p}}}\left(\Delta HKe^{-\frac{Ea_p}{\mathrm{RT}1,m}}+F_{\mathrm{T}}\mathrm{Mwt}_{\mathrm{rg}}c_{\mathrm{prg}}\frac{\left(T_{1,m}-T_{in,m}\right)}{S_r\partial z}+\frac{l_{\mathrm{sfer}}\left(T_{1,m-1}-T_{1,m}\right)}{dr^2}-h_{\mathrm{int}}^{\mathrm{sf}}A_{\mathrm{w}}T_{1,n}\right)\\ 0\end{bmatrix}}_{f(x)}+\begin{bmatrix}0\\ 0\\ \vdots\\ \frac{h_{\mathrm{int}}^{\mathrm{sf}}A_{\mathrm{w}}T_{\mathrm{w}}}{\sum \rho c_p}\\ \vdots\\ 0\\ \frac{h_{\mathrm{int}}^{\mathrm{sf}}A_{\mathrm{w}}T_{\mathrm{w}}}{\sum \rho c_p}\\ \varepsilon\end{bmatrix} \tag{45}$$

The correction term is found in the same way as for the 1-D observer. However, the heat balances are no longer identical for each finite element. Based on the elements within the reactor bed, and not at the wall, Eq. 39 is written

$$\frac{dz}{dX}=\begin{bmatrix}1 & 0\\ \frac{-1}{\sum\left(\rho c_{\mathrm{p}}\right)}\left(\frac{E_a}{\mathrm{RT}^2}Ke^{\frac{-Ea}{\mathrm{RT}}}\Delta H+\frac{F_{in}\mathrm{Mwt}_{\mathrm{g}}cp_{\mathrm{g}}}{S_r dz}+\frac{l_{\mathrm{sfer}}}{dr^2}\right) & \frac{\Delta He^{\frac{-Ea}{\mathrm{RT}}}}{\sum\left(\rho c_{\mathrm{p}}\right)}\end{bmatrix} \tag{46}$$

As this is slightly ambiguous, the 2-D observer was tested with both possible correction terms, that is, derived using Eq. 39 or 31. The observer was programmed with the reactor bed divided into 50 elements, 10 axial, and 5 radial. When the effective conductivity in the bed and the wall heat-transfer coefficient are taken into account separately, the observer calculates the mass of polymer formed in the reactor bed to be 33.2 mg for 33.3 mg measured. Although there is clearly some uncertainty in the accuracy of the measured data and the correlations used, this is a much better result. Testing the observer for other experiments always resulted in accuracy better than 30%. There was no noticeable difference in the results from the two alternative correction terms, which can be explained because the effect is only a slight change to the observer gain, to which the observer is robust.

Figure 9 compares the temperatures predicted by this observer to those calculated by the reactor model (Eqs. 1–17). This observer recalculates the measured data correctly and predicts thermal profiles which are logical and consistent with the trends of the reactor model. Temperatures increase along the reactor length and are cooler at the reactor wall. A small difference can be seen between the predicted edge temperatures in Figure 9b. This can be explained because the reactor wall temperature dynamic is included in the reactor model, whereas it is held constant for the observer. Figure 10 shows the values of $k_{\mathrm{p0}}C_{\mathrm{C2}}C^*$ predicted by the 2-D observer. As before, this parameter is uniform across the reactor bed. The result is slightly less smooth than for the 1-D observer (Figure 7b). This is because the 2-D observer has more reactor elements and so, more temperatures are estimated and the result is noisier. However, the curve is still of the expected form. Note that there is no early minimum in these observer results for $k_{\mathrm{p0}}C_{\mathrm{C2}}C^*$ because the initial value has been set to zero.

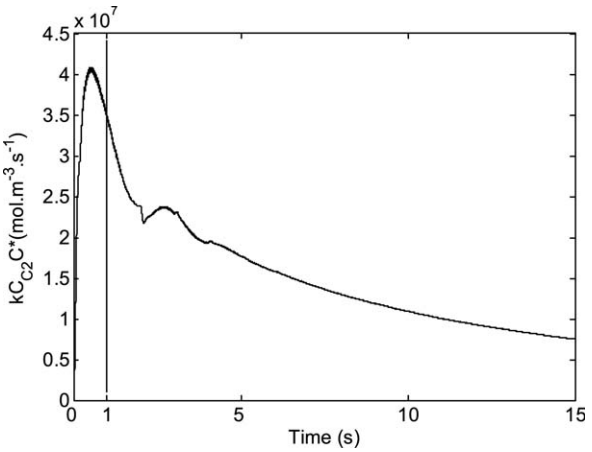

Figure 10. Results of the 2-D observer for $k_{p0}C_{C2}C^*$ with 10 axial and 5 radial bed elements.

Figure 11 compares the reaction rates calculated from the 2-D observer predicted values of $k_{p0}C_{C2}C^*$ to those from the reactor model. Figures 11a, b gives results along the reactor center and edge, respectively. It can be seen that there is reasonable agreement, with the model and the observer predicting similar values and trends. The differences between the estimated and real reaction rates should be due to the simplifications made for development of the observer, in particular, the assumption of T_w, F_T, and ρc_p constant. This simplification was necessary to avoid exhaustive calculations while deriving a canonical form of obsevability. Figure 11 shows that the reaction rates close to the reactor wall are relatively well estimated, but the reaction rates in the reactor center present a higher discrepancy. As with the bed temperatures, the difference in the reaction rates close to the reactor wall can be linked to the reactor wall temperature, which varies in the model but is held constant in the observer. The higher reaction rate in the bed center is more likely to be linked to the assumption of constant gas flow rate.

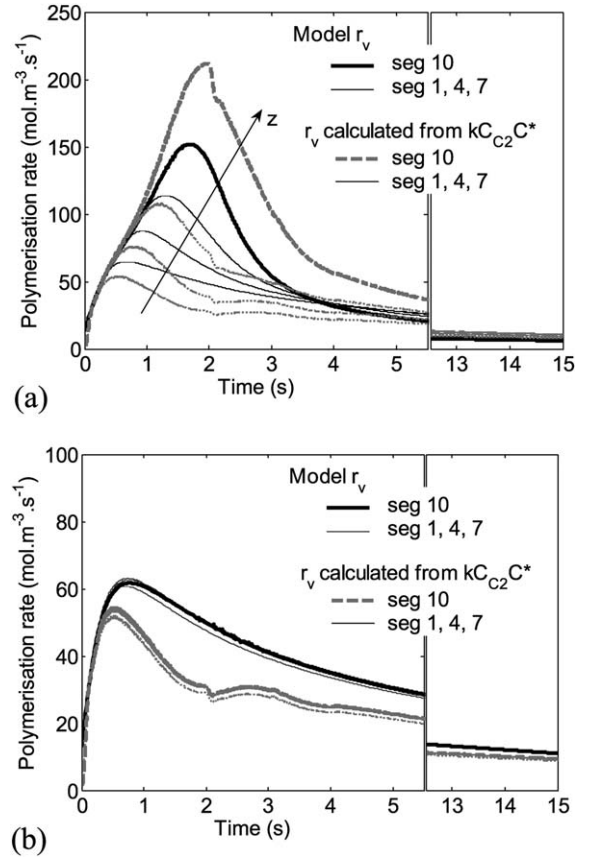

Figure 11. Comparison of reaction rates predicted 2-D observer for $k_{p0}C_{C2}C^*$ with 10 axial and 5 radial bed elements and those calculated by the model at reactor (a) center and (b) edge.

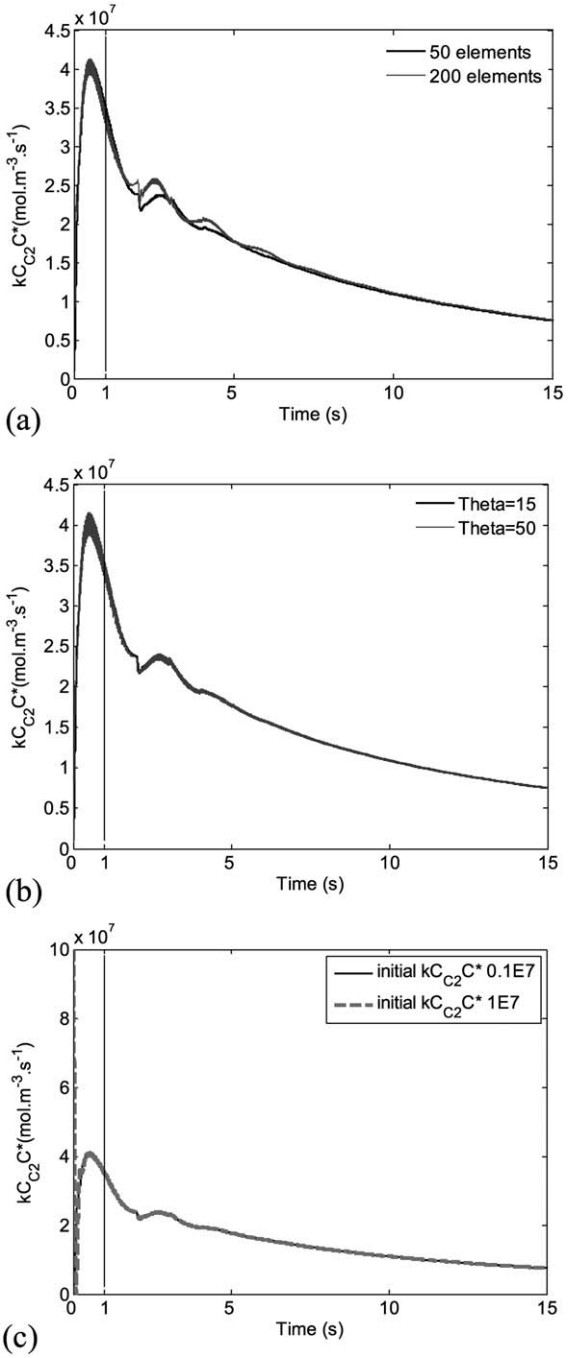

Figure 12. Results of the 2-D observer for $k_{p0}C_{C2}C^*$ with (a) increased number of reactor elements, (b) the tuning parameter, theta, increased to 50, and (c) alternative initial values for $k_{p0}C_{C2}C^*$.

Figure 12 shows the effects of increasing the number of axial elements in the reactor bed, increasing the tuning parameter and changing the initial value of $k_{p0}C_{C2}C^*$. This observer is robust and predicts almost identical results in each case.

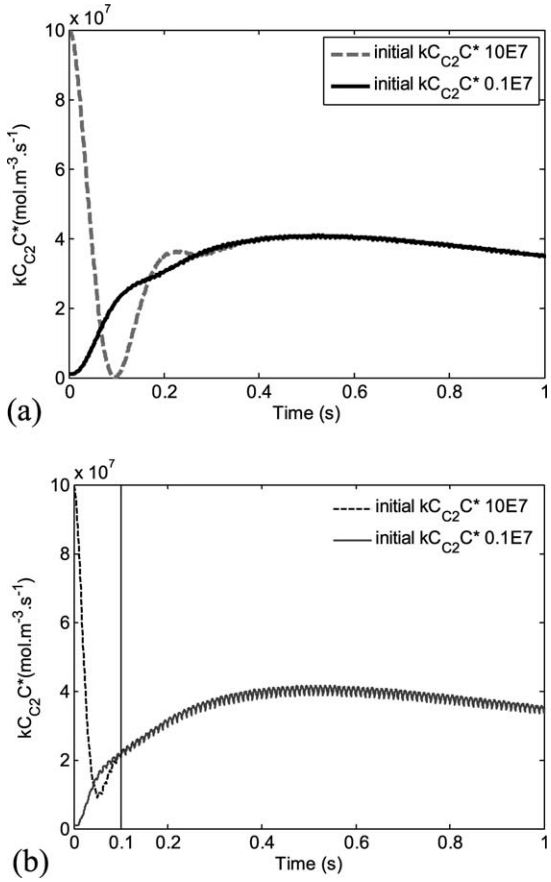

Figure 13. 2-D Observer for $k_{p0}C_{C2}C^*$ with alternative initial values (a) tuning parameter = 15 and (b) tuning parameter = 50.

Figure 13 shows the observer predictions for $k_{p0}C_{C2}C^*$ during the first second with different initial values. It can be seen that even with the tuning parameter set to 50 the observer takes about the first 100 ms of the data to converge, so the predictions before this point must be discarded.

Conclusions

A high gain observer has been developed to estimate reaction rate, distributed both axially and radially, in a stopped flow fixed bed reactor using outlet temperature as the measured variable. The observer is based on the heat balances from a validated model for this reactor and is applied to experiments carried out under controlled conditions. Limiting the operating range of the reactor allowed some simplifications to be made to the heat balances and an initial observer for reaction rate was developed. However, this construction could not be extrapolated to a discretized reactor bed. To overcome this problem, the activation energy for the polymerization was introduced separately to the reaction rate to create an observer for the parameter, K, which was considered uniform across the reactor bed. This method allowed an observer which could estimate all the required states, namely, the temperatures in a distributed system of reactor elements plus the parameter, K. Finally, the wall heat-transfer coefficient was taken into account separately to the radial effective conductivity in the reactor bed to create a 2-D observer which gives reasonably good results.

Observers are usually used for real time process monitoring and control. This work has shown that it is possible to extend an observer to a volume represented by a 2-D system of equations and estimate values of more than 50 separate parameters within this volume. This demonstrates that the observers method can predict useful process information, in very complex systems, which could be of benefit for both research and industrial applications.

Notation

A = state matrix
A_w = wall area for heat transfer per segment volume, $m^2\ m^{-3}$
a,b,c = constants
C = output matrix
C_{C2} = ethylene concentration, mol m^{-3}
C^* = active site concentration, mol m^{-3}
c_p = specific heat capacity, kJ $kg^{-1}\ K^{-1}$
c_{pC2} = specific heat capacity ethylene, kJ $kg^{-1}\ K^{-1}$
D_r = radial Diffusivity, $m^2\ s^{-1}$
d_{reac} = reactor length, m
d_t = reactor diameter, m
Ea_p = activation energy, J mol^{-1}
F_T = total molar flow, mol s^{-1}
h_{bath} = bath side wall heat-transfer coefficient, W $m^{-2}\ K^{-1}$
h_{cat} = catalyst heat-transfer coefficient, W $m^{-2}\ K^{-1}$
h_{int}^{sf} = wall heat-transfer coefficient (2-D model), W $m^{-2}\ K^{-1}$
h_{int} = wall heat-transfer coefficient (1-D model), W $m^{-2}\ K^{-1}$
ΔH = heat of reaction, J mol^{-1}
$H(T)$ = Henry constant for ethylene in polyethylene, $mol^{-1}\ N^{-1}\ m^{-1}$
i = axial element number
k_{p0} = pre-exponential reaction constant for propagation, $mol^{-1}\ s^{-1}\ m^3$
K = lumped reaction constant
l_{reac} = reactor length
l_{f1}, l_{f2} = frit lengths (inlet, outlet)
l_{sfer} = effective bed conductivity, W $m^{-1}\ K^{-1}$
l_{s_inox} = conductivity of stainless steel, W $m^{-1}\ K^{-1}$
L_f = Lie derivative
M_R = mass of polyethylene per unit volume of reactor, g m^{-3}
Mwt_{rg} = molecular weight reaction gas, g mol^{-1}
Mwt_{C2} = molecular weight ethylene, g mol^{-1}
P = pressure, N m^{-2}
R = ideal gas constant, J $mol^{-1}\ K^{-1}$
r = radial distance, m
r_v = apparent reaction rate per unit bed volume, mol $s^{-1}\ m^{-3}$
S_{cat} = catalyst surface area, $m^2\ m^{-3}$
S_r = cross sectional area of segment, m^2
S_θ = explicit solution to Lyapunov equation
T = temperature, K
T_b = wall Temperature, K
T_w = wall Temperature, K
t = time, s
X = state vector
y = measured variable
y_{C2} = mole fraction ethylene
z = state vector after change of variables
z = axial distance, m
Θ = tuning parameter
ε = dynamic to be found by observer
ε_b = bed porosity
ρ = density, kg m^{-3}

Suffixes

c = catalyst & polymer
g = gas & inert solid
rg = reaction gas

Literature Cited

1. GBI Research Reports. Polyethylene market to 2020—North American dominance eroding as polyethylene production shifts to Middle East. 2011: Alacra Store. Available at: http://alacrastore.com/

storecontent/GBI-Research-Reports/Polyethylene-Market-to-2020-North-American-Dominance-Eroding-as-Polyethylene-Production-Shifts-to-Middle-East-2115-195; accessed on April 28, 2014.
2. McKenna TFL, Martino AD, Weickert G, Soares JPB. Particle growth during the polymerisation of olefins on supported catalysts,1—nascent polymer structures. *Macromol React Eng*. 2010;4:40–64.
3. McKenna TF, Soares JBP. Single particle modelling for polyolefins: a review. *Chem Eng Sci*. 2001;56:3931–3949.
4. Olalla B, Broyer JP, McKenna TFL. Heat transfer and nascent polymerisation of olefins on supported catalysts. *Macromol Symp*. 2008;271:1–7.
5. Tioni E, Spitz R, Broyer JP, Monteil V, McKenna TFL. Packed-bed reactor for short time gas phase olefin polymerization: heat transfer study and reactor optimisation. *AIChE J*. 2012;58:256–267.
6. Browning B, Pitault I, Sheibat-Othman N, Tioni E, Monteil V, McKenna TFL. Dynamic modelling of a stopped flow fixed bed reactor for gas phase olefin polymerisation. *Chem Eng J*. 2012;207–208:635–644.
7. Vazquez R, Schuster E, Krstic M. Magnetohydrodynamic state estimation with boundary sensors. *Automatica*. 2008;44:2517–2527.
8. LeBreux M, Désilets M, Lacroix M. An unscented Kalman filter inverse heat transfer method for the prediction of the ledge thickness inside high-temperature metallurgical reactors. *Int J Heat Mass Transfer*. 2013;57:265–273.
9. Aguilar-Garnica E, Garcia-Sandoval JP, Gonzalez-Figueredo C. A robust monitoring tool for distributed parameter plug flow reactors. *Comput Chem Eng*. 2011;35:510–518.
10. Dochain D. State observers for tubular reactors with unknown kinetics. *J Process Control*. 2000;10:259–268.
11. Hua X, Mangold M, Kienle A, Gilles ED. State profile estimation of an autothermal periodic fixed-bed reactor. *Chem Eng Sci*. 1998;53:47–58.
12. Wu HN, Li HX. Robust adaptive neural observer design for a class of nonlinear parabolic PDE systems. *J Process Control*. 2011;21;1172–1182.
13. Mangold M, Buck A, Schenkendorf R, Steyer C, Voigt A, Sundmacher K. Two state estimators for the barium sulfate precipitation in a semi-batch reactor. *Chem Eng Sci*. 2009;64:646–660.
14. Edouard D, Sheibat-Othman N, Hammouri H. Observer design for particle size distribution in emulsion polymerization. *AIChE J*. 2005;51:3167–3185.
15. Zhang K, Nadri M, Xu CZ. Reachability-based feedback control of crystal size distribution in batch crystallization processes. *J Process Control*. 2012;22:1856–1864.
16. Vande Wouwer A, Point N, Porteman S, Rémy M. An approach to the selection of optimal sensor locations in distributed parameter systems. *J Process Control*. 2000;10:291–300.
17. Alonso AA, Kevrekidis IG, Banga JR, Frouzakis CE. Optimal sensor location and reduced order observer design for distributed process systems. *Comput Chem Eng*. 2004;28:27–35.
18. Kreuzinger T, Bitzer M, Marquardt W. State estimation of a stratified storage tank. *Control Eng Pract*. 2008;16:308–320.
19. Perry RH, Green DW. *Perry's Chemical Engineers' Handbook*, 7th ed. New York: McGraw Hill, 1997.
20. Reid RC, Prausnitz JM, Poling BE. *The Properties of Gases & Liquids*, 4th ed. New York: McGraw Hill, 1987.
21. Kunii D, Levenspeil O. *Fluidisation Engineering*. New York: Wiley, 1969.
22. Specchia V, Baldi G, Sicardi S. Heat transfer in packed bed reactors with one phase flow. *Chem Eng Commun*. 1980;4:361–380.
23. Kunii D, Smith J.M. Heat transfer characteristics of porous rocks. *AIChE J*. 1960;6:71–78.
24. Yagi S, Kunii D, Wakao N. Studies on axial effective thermal conductivities in packed beds. *AIChE J*. 1960;6:543–546.
25. Maxwell JC. *Electricity and Magnetism*. Oxford UK: Clarendon Press, 1873.
26. Rincon FD, Esposito M, de Araujo PHH, Sayer C, Le Roux GAC. Studies calorimetric estimation employing the unscented Kalman filter for a batch emulsion polymerization reactor. *Macromol React Eng*. 2013;7:24–35.
27. Sheibat-Othman N, Othman S. Control of an emulsion polymerization reactor. *Ind Eng Chem Res*. 2006;45:206–211.
28. Alamir M, Sheibat-Othman N, Othman S. Constrained nonlinear predictive control for maximizing producion in polymerzation processes. *IEEE Trans Control Syst Technol*. 2007;15:315–323.
29. Gauthier JP, Bornard G. Observability for any u(t) of a class of bilinear systems. *IEEE Trans Automat Control*. 1981;26,922–926.
30. Gauthier JP, Hammouri H, Othman S. A simple observer for nonlinear systems. Application to bioreactors. *IEEE Trans Automat Control*. 1992;37,875–880.
31. Froment GF. Fixed bed catalytic reactors. *Ind Eng Chem*. 1967;59:18–27.

Manuscript received Jan. 10, 2014, and revision received May 30, 2014.